Physics of Plasmas

ICRF fast wave current drive and mode conversion current drive in EAST tokamak

Cite as: Phys. Plasmas **24**, 102502 (2017); https://doi.org/10.1063/1.5002137
Submitted: 04 May 2017 . Accepted: 27 August 2017 . Published Online: 18 September 2017

L. Yin, C. Yang, X. Y. Gong, X. Q. Lu, D. Du, and Y. Chen

View Online Export Citation CrossMark

ARTICLES YOU MAY BE INTERESTED IN

Validation of the model for ELM suppression with 3D magnetic fields using low torque ITER baseline scenario discharges in DIII-D
Physics of Plasmas **24**, 102501 (2017); https://doi.org/10.1063/1.5000276

The sensitivity of tokamak magnetohydrodynamics stability on the edge equilibrium
Physics of Plasmas **24**, 102503 (2017); https://doi.org/10.1063/1.4986036

Destabilization of beta-induce Alfvén eigenmodes by energetic trapped ions in low-magnetic-shear plasma
Physics of Plasmas **24**, 102114 (2017); https://doi.org/10.1063/1.4996605

© 2017 Author(s).

ICRF fast wave current drive and mode conversion current drive in EAST tokamak

L. Yin,[1,2] C. Yang,[3] X. Y. Gong,[2,a)] X. Q. Lu,[2] D. Du,[1] and Y. Chen[1,2]
[1]School of Mathematics and Physics, University of South China, Hengyang 421001, China
[2]School of Nuclear Science and Technology, University of South China, Hengyang 421001, China
[3]Institute of Plasma Physics, Chinese Academy of Sciences, Hefei 230031, China

(Received 4 May 2017; accepted 27 August 2017; published online 18 September 2017)

Fast wave in the ion-cyclotron resonance frequency (ICRF) range is a promising candidate for non-inductive current drive (CD), which is essential for long pulse and high performance operation of tokamaks. A numerical study on the ICRF fast wave current drive (FWCD) and mode-conversion current drive (MCCD) in the Experimental Advanced Superconducting Tokamak (EAST) is carried out by means of the coupled full wave and Ehst-Karney parameterization methods. The results show that FWCD efficiency is notable in two frequency regimes, i.e., $f \geq 85$ MHz and $f = 50$–65 MHz, where ion cyclotron absorption is effectively avoided, and the maximum on-axis driven current per unit power can reach 120 kA/MW. The sensitivity of the CD efficiency to the minority ion concentration is confirmed, owing to fast wave mode conversion, and the peak MCCD efficiency is reached for 22% minority-ion concentration. The effects of the wave-launch position and the toroidal wavenumber on the efficiency of current drive are also investigated. *Published by AIP Publishing.* [http://dx.doi.org/10.1063/1.5002137]

I. INTRODUCTION

The fast wave (FW) in the ion cyclotron resonance frequency (ICRF) range is an essential method for heating magnetically confined plasmas. It can also be used to supply non-inductive current for tokamaks and improve confinement performance by modifying the current profile.[1–4] Compared with the other current-drive (CD) methods, such as electron cyclotron current drive (ECCD) and lower hybrid current drive (LHCD), the fast wave can ensure highly efficient current drive on the magnetic axis and is of low cost.[5] In the ion-ion hybrid resonance layer of a multi-species plasma, fast waves can convert into short-wavelength ion Bernstein waves (IBW) and ion cyclotron waves (ICW) that are efficient for current driving.[6,7] For effective current drive, most wave power must be deposited on electrons through single-pass absorption by electron Landau damping and transit time magnetic pumping.[8] In addition, the coupling problem of RF power from the antenna to plasma in the ICRF system is being solved.[9]

Fast wave current drive (FWCD) and mode-conversion current drive (MCCD) experiments have been widely performed on the DIII-D, ASDEX Upgrade, TFTR, and other tokamaks.[6,10–13] Electron heating and current drive on the DIII-D by the fast wave have been demonstrated, and it was found that the FWCD efficiency increases linearly with the electron temperature, in agreement with the theory.[10–12] In subsequent studies, solely non-inductive current drive was achieved with a combination of FWCD and ECCD. The FWCD efficiency has been calculated by using a ray tracing method. Furthermore, fast wave on-axis current drive and off-axis mode-converted waves(MCW) current drive in D(^{3}He) plasma were conducted on the ASDEX Upgrade.[13] FWCD and MCCD are more promising for ITER and future reactors since single-pass damping in these plasmas will be much higher because of their larger size and higher densities and temperatures. Accordingly, how to enhance the single-pass absorption of the fast and mode-converted waves and the current drive efficiency should still be investigated.

ICRF wave heating/current system is equipped in EAST tokamak.[14] It contains eight RF transmitters with an output power up to 12.0 MW (1.5 MW each), and can provide a wave with the frequency range from 30 MHz to 110 MHz. The main purpose of the ICRF on the EAST is to study on-axis and off-axis heating schemes for ions and electrons.[15–17] The main current drive method on the EAST is lower hybrid current drive; however, high density and temperature can limit the penetration of LH waves into the core plasma.[18–21] The H-mode experiments with the 2.45 GHz LHCD system have shown that current drive efficiency decreases sharply at high density due to parametric instability and collisional absorption in the edge region.[22] By contrast, the fast wave in the ICRF can easily penetrate into the centre of high-density plasma, providing central current drive without limits on accessibility. Therefore, as an attractive supplementary current drive method, the simulation studies of the absorption and current drive physics of fast wave in the ICRF should be conducted so as to facilitate the plan and analysis of experiments on the EAST. In this paper, we shall investigate FWCD and MCCD in order to enhance single-pass absorption of FW and MCW and maximise current drive efficiency on EAST.

The remainder of this paper is organized as follows. The FW propagation and absorption model and research method are introduced in Sec. II. The numerical analysis for optimising FWCD and MCCD in EAST discharges is presented in Sec. III. Some brief conclusions are drawn in Sec. IV.

II. FULL-WAVE METHOD AND EHST-KARNEY (EK) PARAMETRIZATION

A. Full-wave model

For the simulation of FWCD and MCCD in the ion cyclotron range of frequencies, a ray-tracing method[23]

a)Author to whom correspondence should be addressed. Electronic mail: gongxueyu@126.com

cannot be adopted since the wavelength is comparable to the size of EAST, hence a full-wave method[24–27] should be employed. The full-wave codes used commonly include PION, AORSA, PICES, and TORIC[28] at present. The code TORIC, in particular, offers a satisfactory full-wave solution of Maxwell-Vlasov equations, concerning hot plasmas in an arbitrary axisymmetric toroidal geometry, and provides reliable physics for ion cyclotron wave propagation and absorption. Moreover, the special effects of toroidicity on wave absorption and mode conversion are also considered. The code has been benchmarked with other ICRF codes and experiments and has proven to be a useful tool.[28–34] The TORIC code is used in combination with the Ehst-Karney (EK) formula to simulate the physics of FWCD and MCCD for the EAST in this paper. The code describes dissipative effects including absorption by the electrons through Landau damping and transit-time magnetic pumping, and by the ions at the cyclotron frequency and its first harmonic.[32]

TORIC solves the Maxwell wave equation given by

$$\nabla \times \nabla \times \vec{E} - \frac{w^2}{c^2}\left(\vec{E} + \frac{i\mu_0 c^2}{w}\left(\vec{J}^{(P)} + \vec{J}^{(A)}\right)\right) = 0, \quad (1)$$

where $\vec{J}^{(P)}$ and $\vec{J}^{(A)}$ are the plasma and antenna currents, respectively. The wave equation is derived from the Vlasov equation by expanding the electromagnetic fields in Fourier modes in the toroidal and poloidal angles φ, θ using the formula

$$\vec{E}(x) = \sum_{m,n} \vec{E}_m(r) \exp\left(im\theta + in\phi\right), \quad (2)$$

where m and n refer to the poloidal and toroidal mode number, respectively. The plasma current $\vec{J}^{(P)}$ can be written as an integration over the wave electric field $\vec{E}$. In the ion cyclotron range of frequencies, it is justifiable to use the finite Larmor radius approximations,[35] namely,

$$\vec{J}^{P} = \vec{J}^{(0)} + \vec{J}^{(2)} \quad \vec{J}^{(2)} = \vec{J}_i^{(2)} + \vec{J}_e^{(2)}, \quad (3)$$

where the superscript 0 and 2 denote the orders in the current expansion over Larmor radius. Large Larmor radius effects are taken into account in order to describe ion Bernstein waves (IBW) excited by mode conversion.[36] In the numerical approach, there is a spectral representation of the solution in the poloidal angle θ and cubic finite elements in the radial variable ψ. These numerical methods provide an accurate evaluation of the electromagnetic field and the power deposition profiles in a toroidal geometry. Various contributions to Pabs(ψ) are enumerated, such as the fundamental ion cyclotron absorption

$$P_{\mathrm{i}}^{1} = \frac{\omega}{4\pi}\mathrm{Re}\sum_{m}\sum_{m'}\int RJ_{\mathrm{p}}\mathrm{e}^{\mathrm{i}(m'-m)\vartheta} \times \left\{E_{+}^{(m)*}(\psi)\mathrm{Im}\left(\mathrm{L}\left(\psi,,\vartheta,\mathrm{k}_{\zeta}^{m'}\right)\right)E_{+}^{(m')}(\psi)\right\}d\theta \quad (4)$$

the ion second-harmonic absorption

$$P_{\mathrm{i}}^{2}(\psi) = -\frac{\omega}{8\pi}\mathrm{Re}\sum_{m,m'}\frac{c^2}{\omega^2}\int RJ_{\mathrm{p}}\mathrm{e}^{\mathrm{i}(m'-m)\vartheta} \times \left\{\nabla_{\perp}\cdot\left(\mathrm{R}\cdot E_{\perp}^{m} + \mathrm{i}u_{\zeta}\times\mathrm{R}\cdot E_{\perp}^{m}\right)^{*} \times \mathrm{Im}\left(\hat{\lambda}_{\mathrm{i}}^{(2)}\left(\psi,\vartheta;k_{\zeta}^{m\prime}\right)\right)\cdot\nabla_{\perp} \times\left(\mathrm{R}\cdot E_{\perp}^{m}+\mathrm{i}u_{\zeta}\times\mathrm{R}\cdot E_{\perp}^{m}\right)\right\}\mathrm{d}\vartheta \quad (5)$$

the electron Landau damping

$$P_{\mathrm{e}}^{0}(\psi) = \frac{\omega}{4\pi}\mathrm{Re}\sum_{\mathrm{m}}\sum_{m'}\int RJ_{\mathrm{p}}\mathrm{e}^{\mathrm{i}(m'-m)\vartheta} \times\left\{E_{\zeta}^{(m)*}(\psi)\mathrm{Im}\left(\mathrm{P}\left(\psi,\vartheta,\mathrm{k}_{\zeta}^{m'}\right)\right)E_{\zeta}^{(m')}(\psi)\right\}\mathrm{d}\vartheta \quad (6)$$

and the electron transit-time damping

$$P_{\mathrm{e}}^{\mathrm{TT}}(\psi) = -\frac{\omega}{4\pi}\mathrm{Re}\sum_{m,m'}\frac{c^2}{\omega^2}\int RJ_{\mathrm{p}}\mathrm{e}^{\mathrm{i}(m'-m)\vartheta} \times\left\{\left(\nabla_{\perp}\times E_{\perp}^{m}\right)^{*}\cdot\mathrm{Im}\left(2\hat{\lambda}^{0}\left(\psi,\vartheta;k_{\zeta}^{m'}\right)\right)\cdot \times\left(\nabla_{\perp}\times E_{\perp}^{m'}\right)\right\}\mathrm{d}\vartheta. \quad (7)$$

B. Ehst-Karney parametrization

In an axisymmetric tokamak in steady equilibrium without an inductive electric field, the current parallel to the magnetic field can be expressed as[37]

$$\mathrm{j}_{||} = \mathrm{j}_{||}^{\mathrm{PS}} + \mathrm{B}(\mathrm{G}+\mathrm{H}), \quad (8)$$

where $j_{//}^{PS}$ is the well-known Pfirsch-Schlüter current, B is the magnetic field strength, H is the bootstrap current, and G is the non-inductive current.

Certain simplifications are assumed when performing the velocity space integration over a response function χ[38] which is

$$\chi = \left[1-(\lambda_t/\lambda)^{\alpha}\right]2\omega u^3/(5+Z_{eff}), \quad (9)$$

where ω and x are the parallel and perpendicular velocity components of electrons normalised to the thermal speed, respectively, wherein the normalised speed is $u=(x^2+\omega^2)^{1/2}$, and $\lambda = \omega/u$ is the pitch angle. If B_M is the maximum field amplitude on a flux surface, trapped electrons exhibit $0<\lambda<\lambda_{\mathrm{t}}$, where $\lambda_t^2 = 1-(B/B_M)$. The passing electrons have $x<x_t$, where $x_t \equiv \omega(B/B_M)^{1/2}[1-(B/B_M)]^{1/2}$. On a given poloidal flux surface ψ, the RF-driven current density, taking into account the effect of electromagnetic trapping, is expressed as

$$G(\psi) = \langle \mathrm{j}_{||}^{\mathrm{RF}}\mathrm{B}\rangle/\langle \mathrm{B}^2\rangle = \frac{V'}{\mathrm{L}}\eta\langle \mathrm{p}^{\mathrm{RF}}\rangle, \quad (10)$$

where $\mathrm{V}' = \mathrm{dV}/\mathrm{d}\psi$ is the derivative of the toroidal volume with respect to the poloidal flux, P^{RF} is the RF heating power density, and $\langle\rangle$ denotes the flux surface average. In normalisation, the current drive efficiency is related to a dimensionless function

$$\eta = \frac{j_{//}^{RF}}{P^{RF}} = \frac{38.4 \times 10^{18}\,\mathrm{T_e}}{\ell \mathrm{n}\,\Lambda\ \mathrm{n_e}}\tilde{\eta}, \tag{11}$$

where $\ell n\Lambda$ is the Coulomb logarithm, n_e is the local electron density. A uniform approximation of the efficiency is

$$\tilde{\eta} = \mathrm{CM}\eta_0 R, \tag{12}$$

with

$$C = 1 - \exp\left(-\left(cx_t^2\right)^m\right), \tag{13}$$

$$M = 1 + a(\lambda_t/\omega)^k, \tag{14}$$

$$R = 1 - \frac{\varepsilon^n\sqrt{x_r^2+\omega^2}}{\varepsilon^n x_r + \omega}, \tag{15}$$

$$\eta_0 = \frac{K}{\omega} + D + \frac{4\omega^2}{5+Z_{eff}} \tag{16}$$

where C is the linearised electron collision operator, Z_{eff} is the ion effective charge, ε is the inverse aspect ratio, K and D are functions of Z_{eff}, and K, D, m, c, a, k, n are experience values. Formula (11) can be used, together with the power deposition on the magnetic surface which is obtained by TORIC, to calculate the driving current.

III. OPTIMUM CALCULATIONS FOR FWCD AND MCCD IN EAST DISCHARGES

The EAST equilibrium used here for TORIC was reconstructed by using the EFIT code and applying the constraints from experimental diagnostics in D(H) discharge #62946 at 2.8 s, with a toroidal magnetic field of $B_0 = 2.57$ T and a plasma current of 0.5 MA. The majority ion species was deuterium, with 1.6% minority ion fraction of hydrogen. The flux surfaces of the equilibrium are given in Fig. 1(a). The profiles of the plasma density and temperature shown in Figs. 1(b) and 1(c) were also obtained from experimental diagnosis.

A. Wave frequency

Ion cyclotron damping of the fast wave of frequencies over 30 MHz was very efficient in the EAST experiments. However, FWCD in ICRF relies on electron absorption to drive the toroidal non-inductive current, it is necessary to tune the ICRF system in order to ensure that the majority of the total wave power is directly absorbed by electrons rather than ions. For the standard mid-plane launch, an appropriate frequency was selected from the ICRF, so as to avoid ion cyclotron resonances located on the low-field side (LFS). Figure 2 shows the location of the resonance layer for the fundamental and second-harmonics of H ions, and the

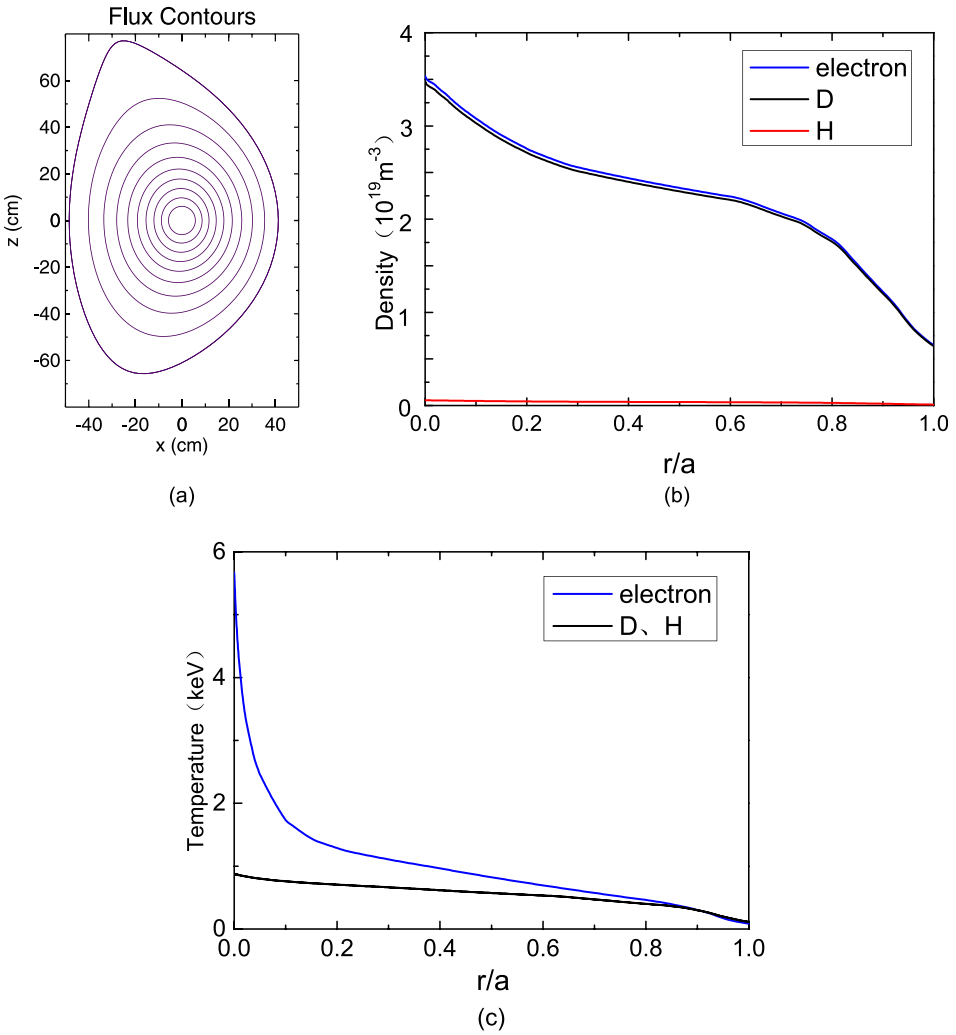

FIG. 1. (a) An EAST equilibrium with $B_0 = 2.57$ T and $I_p = 500$ kA; (b) the profile of the plasma density; and (c) the profile of the plasma temperature.

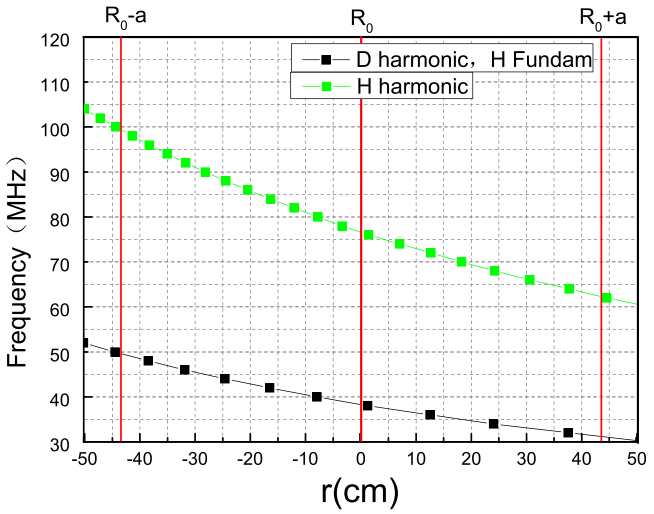

FIG. 2. Locations of the (1st and 2nd) resonance layers for H and D ions with waves of frequencies from 30 MHz to 110 MHz in the EAST.

second harmonic of D ions at wave frequencies from 30 MHz to 110 MHz in EAST, wherein two frequency regimes of dominant electron absorption with potential for efficient CD can immediately be identified, namely, $f \geq 85$ MHz for which second-harmonic H ion absorption occurs on the high-field side (HFS), and $f = 50$–65 MHz for which there are none resonances of ions inside the plasma.

Figure 3 shows corresponding absorbed power fractions of the plasma species as a function of wave frequency for a single toroidal mode number $n_\phi = 23$. The results indicate that over 90% of the total power is absorbed by electrons through Landau damping and transit-time magnetic pumping in the two frequency ranges, namely, $f \geq 85$ MHz and $f = 50$–65 MHz for which ion absorption is avoided. The RF power is mainly absorbed via H ion fundamental cyclotron damping in the frequency range of 30 MHz to 50 MHz, and the power absorbed via H ion second-harmonic damping is roughly equivalent to that absorbed by electrons in the frequency range of 65 MHz to 85 MHz. The Doppler effect substantially broadens the width of the ion cyclotron absorption region in these cases.

Figure 4 shows the current drive (CD) efficiency as a function of the wave frequency. The results indicate that the

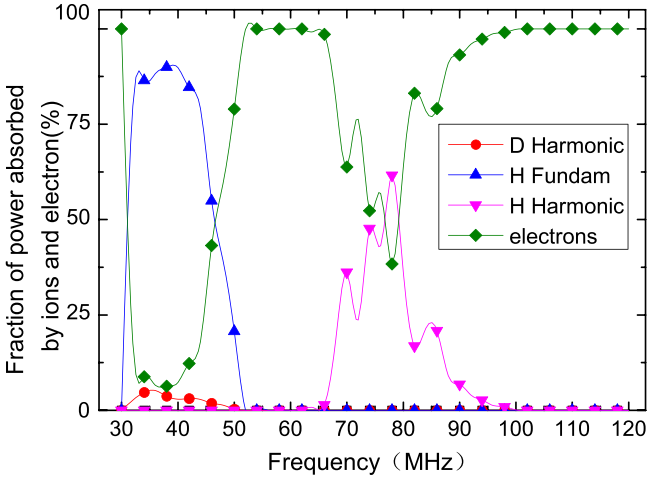

FIG. 3. Absorbed power fractions of electrons and two ions, plotted against wave frequency.

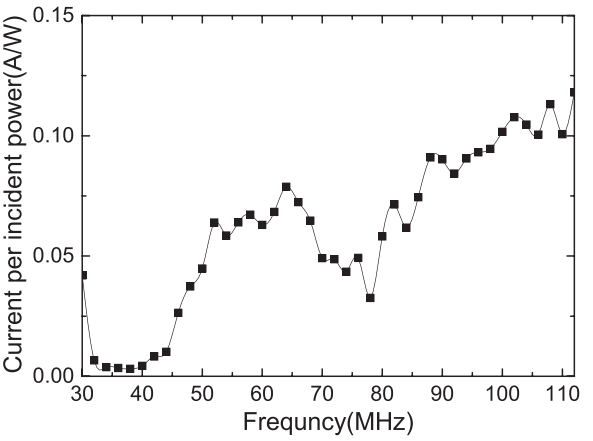

FIG. 4. The driven current per unit power versus wave frequency.

CD efficiency is notable in two frequency regimes, namely, $f \geq 85$ MHz and $f = 50$–65 MHz. This is consistent with the results on the frequency regimes of effective electron absorption shown in Fig. 3. The CD efficiency is up to 0.12 A/W(120 kA/MW), which is comparable to the plasma current in the experiment on EAST. In addition, Fig. 4 also shows the CD efficiency increase as the fast wave frequency increases in the frequency regimes of effective electron absorption, because the driven current per unit incident power is dependent not only on the electron absorption but also the local current drive efficiency. High wave frequency means high wave parallel phase velocity $v_{//\mathrm{ph}} = \omega/k_{//}$ for a fixed parallel wave number, and then the wave is resonant with and accelerates the passing electrons with higher velocities. Thus, the local current drive efficiency increases.

Figure 5 presents the radial profile of the driven current at 38 MHz, 56 MHz, 80 MHz and 100 MHz. It shows that 90% of the generated current is localized centrally, within $0 \leq \rho \leq 0.1$ owing to the single-pass absorption in the high temperature and density core plasmas of EAST. The results are similar to that from simulations and experiments on other tokamaks.[39,40]

B. Minority ion concentration

In D(H) discharge experiments, fast waves in the ICRF can convert into short-wavelength IBW, which propagate towards to the high-field side, and ICW, which propagate

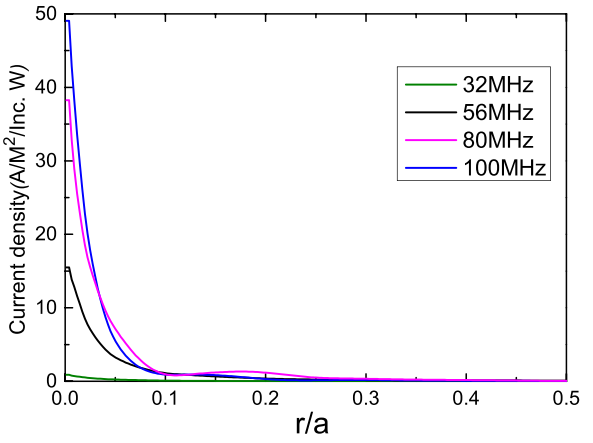

FIG. 5. The radial profiles of the driven current at 38 MHz, 56 MHz, 80 MHz, and 100 MHz.

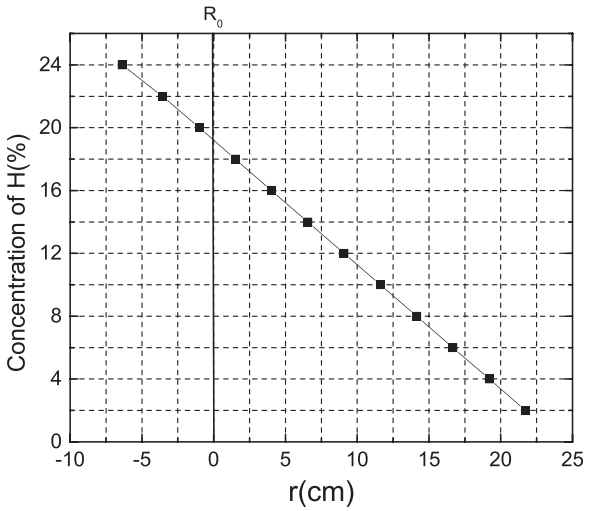

FIG. 6. Locations of the ion-ion hybrid resonance layer with the H minority ion concentration from 2% to 24% for $f = 34$ MHz.

back the low-field side. The mode conversion relate to the minority ion concentration. By applying the H-puff of the variable gas injection rate before the RF power injection, the concentration of H (minority ions) varies. For the case with the wave frequency is 34 MHz, with the H 1st and D 2nd resonance layer located at $x = 24.206$ cm (where x is the distance from the centre of plasma in the equatorial plane) on the low-field side, the ion heating scenario is dominant. As H concentration increases, the ion-ion hybrid resonance layer moves from the low-field side towards the high-field side, as shown in Fig. 6. Therefore, the distance between the hydrogen resonance layer and the mode conversion layer increases, and the backward propagating wave ICW is significantly absorbed by electrons through Landau damping, and cannot propagate to the resonance region of H ions over a long distance. In addition, the wave electric field component E_+, rotating in the same direction as that of the ions and being important for H minority damping, is reduced near the ion cyclotron resonance layer when the minority ion concentration is high enough. As a result, the ions damping is weakened, and the power on the electrons increases as shown in Fig. 7.

Figure 7 presents the power fractions absorbed by the plasma species for minority ion concentrations of between

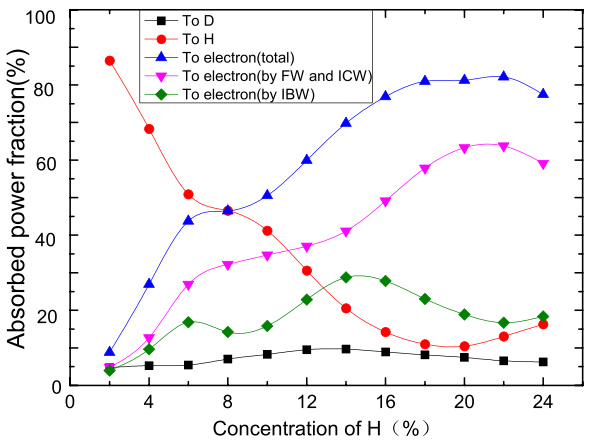

FIG. 7. Absorbed power fractions versus the minority ion concentration for $f = 34$ MHz.

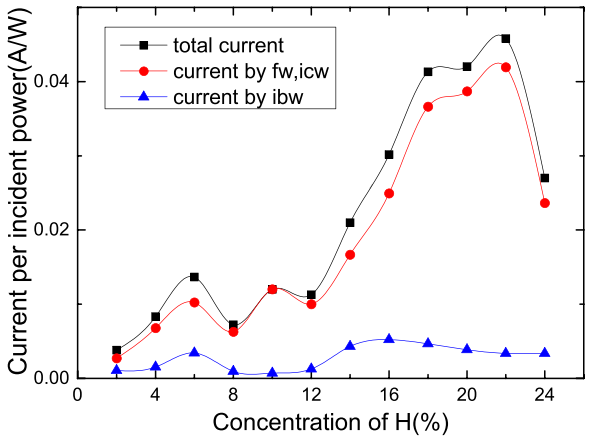

FIG. 8. The driven current per unit power, plotted against the minority ion concentration, at $f = 34$ MHz.

2% and 24% at a wave frequency of 34 MHz. The electron absorption becomes dominant and reaches a maximum of 83.57% for an H concentration of 22%, owing to the mode conversion, when the minority ion concentration is above 10%. The mode conversion layer is located near the center of the plasma ($x = -3.563$ cm) at a high temperature in this case.

As shown in Fig. 8, the driven current per unit power increases and reaches the maximum 47 kA/MW at H concentration of 22% when the minority ion concentration increases. However, beyond the optimum H concentration for ICRF mode conversion, the single-pass mode conversion damping decreases and the value of MCCD efficiency also diminishes if the H concentration increases further.

C. Optimization of the poloidal position of the central point of the antenna

The ICRF wave infection adopts a standard mid-plane launch from the low field. The ion cyclotron resonance layer is at the low-field side (LFS) edge which is situated in front of the electron absorption region in most cases. Ion heating is the main competition for effective absorption of electrons. The alternative option depends on an "upper port" launch position above the mid-plane, from which the launching wave may avoid propagating into the ion heating region. This can enhance the potential of electron absorption and FWCD.

It is clearly shown in Fig. 9 that the best poloidal angle for launching FW at a frequency of 32 MHz is 60° above the outer equatorial plane. The optimum current drive efficiency is six times that of the preceding value. Figure 10 shows the radial profiles of the driven current for 0°, 30°, 60°, and 90°, respectively, from the outer equatorial plane. The simulation results confirm that the launching wave can avoid propagating in the ion heating region for an appropriate "upper port" launch in this case.

There is no substantial improvement of current drive efficiency from an "upper port" launch for a wave frequency of 96 MHz as shown in Fig. 11. The reason is that the ion cyclotron resonance layer is at the high-field side (HFS) and most of the wave power is absorbed by electrons before

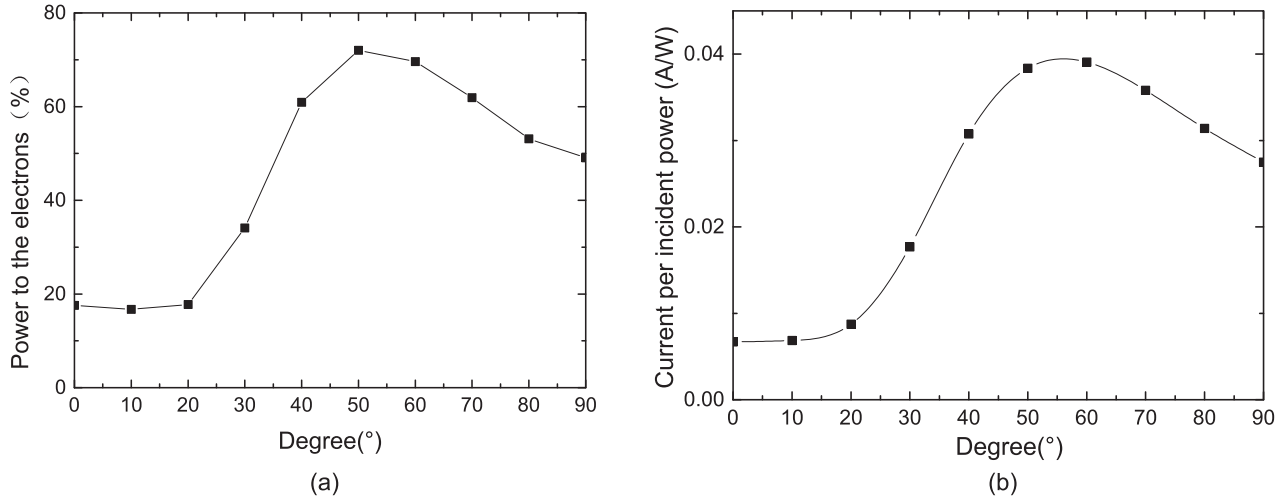

FIG. 9. (a) The power fraction absorbed by electrons versus the wave injection angle above the outer equatorial plane, at 32 MHz, and (b) the driven current per unit power versus the wave injection angle above the outer equatorial plane, at 32 MHz.

reaching the ion cyclotron resonance layer for this wave frequency.

The results encourage an in-depth assessment of this option for fusion reactor application.

D. Toroidal wavenumber

Figure 12 shows the CD efficiency as a function of the toroidal wavenumber N_ϕ for $f = 62$ MHz and $f = 90$ MHz. The CD efficiency initially increases up to a peak, then decreases before levelling out as N_ϕ increases. Electron Landau damping is most efficient when the parallel wave phase velocity $v_{//ph} = \omega/k_{//} (k_{//} \approx N_\phi/R)$ matches the thermal velocity of the electrons. The largest electron absorption occurs at $v_{//ph}/v_{the} = 0.7$ for FW in the ICRF. Thus, the parallel wave phase velocity, which is greater than electron thermal velocity, decreases and approaches the electron thermal velocity, then more power is absorbed by electrons, and CD efficiency is enhanced when N_ϕ increases. Conversely, as already mentioned in Sec. III A, the driven current per unit incident power is also relevant to local current drive efficiency, decreasing sharply as N_ϕ increases (lower $v_{//ph}$) for the electron trapping effect. The point of maximum CD efficiency marks a good compromise between these two factors. The antenna should be designed to make the launch spectrum having its peak at an appropriate toroidal wavenumber.

The peaks of CD efficiency occur at $N_\phi = 8$ for $f = 62$ MHz and at $N_\phi = 24$ for $f = 90$ MHz. Because wave frequency also influences the parallel wave phase velocity, N_ϕ needs to be adapted for a given project in order to achieve the optimum choice for maximising the driven current.

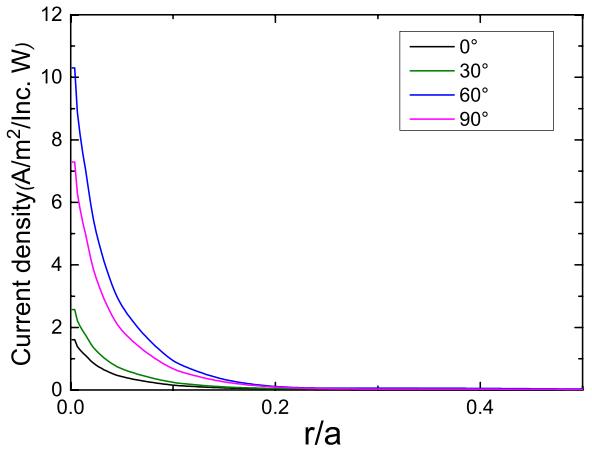

FIG. 10. Radial profiles of the driven current for different angles from the outer equatorial plane.

IV. CONCLUSIONS

Based on the real discharges, the numerical simulations of the physics and optimum performance of FWCD and MCCD in the ion cyclotron range of frequencies in the EAST have been performed by means of the coupled full wave and Ehst-Karney parameterization methods. The results show that FWCD efficiency is notable in two frequency regimes, namely, f ≥ 85 MHz and $f = 50$–65 MHz, for which the ion cyclotron absorption is effectively avoided. The maximum driven on-axis current per unit power can reach 120 kA/MW which is comparable to the plasma discharge current in experiment on EAST. The CD efficiency was found to be sensitive to the minority ion concentration and reaches its maximum at an H concentration of 22% owing to fast wave mode conversion, where the mode conversion layer moves from the low-field side to the centre of the plasma, and more power from RF waves tends to be absorbed by single-pass electrons.

It was found that an "upper port" launch position above the mid-plane can greatly enhance the potential of CD. The optimal "upper port" launch position is 60° from the outer equatorial plane for FWCD, from which the launching waves avoid propagating into the ion heating region.

Finally, the simulation results also show the influence of the toroidal wavenumber on the CD efficiency. The CD efficiency initially increases up, then decreases as Nϕ increases. The maximum CD efficiency marks a good compromise between the electron absorption and the local current drive efficiency. It is necessary to design the antenna to make the launch spectrum has its peak in the optimized region.

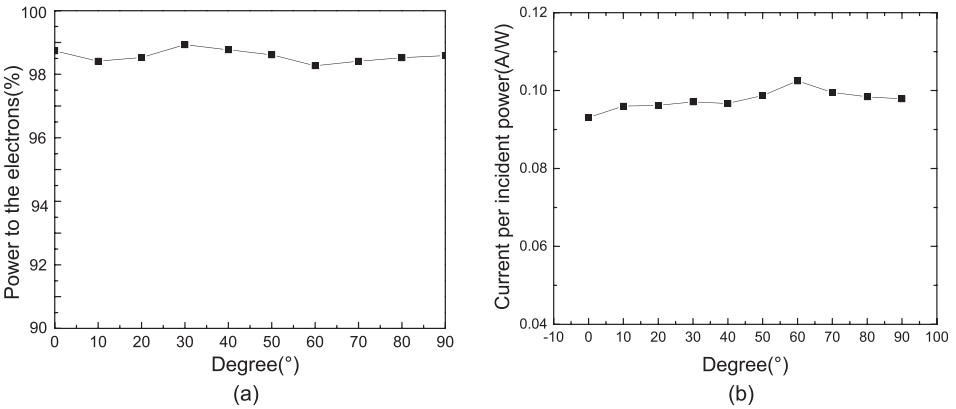

FIG. 11. (a) The power fraction absorbed by electrons versus the wave launch angle from the outer equatorial plane for FW of 96 MHz; (b) the driven current per unit power versus the wave launch angle from the outer equatorial plane for FW of 96 MHz.

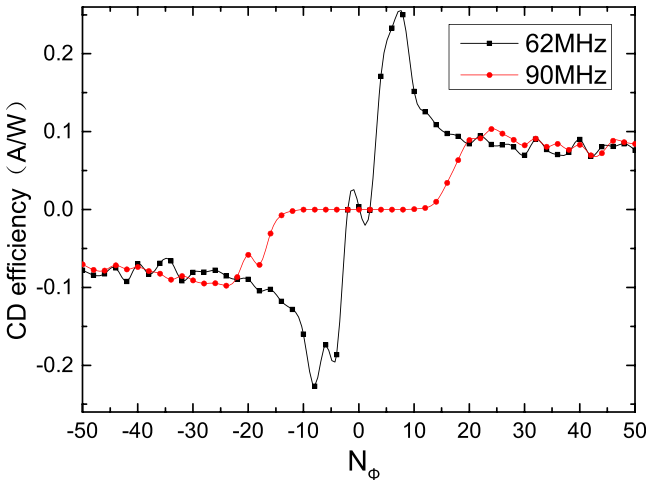

FIG. 12. CD efficiencies as a function of N_ϕ for $f = 62$ MHz (black) and $f = 90$ MHz (red).

The results of our study confirm that the ICRF system, in addition to its significance in heating the plasma, is a competitive candidate for non-inductive current drive in tokamaks such as EAST. FW in the ICRF can provide efficient on-axis current while the lower hybrid waves often drive off-axis current. The simulation study on physics and optimal performance of FWCD and MCCD facilitate the planning and analyzing of experiments on EAST. This work is also helpful to the plan of ion cyclotron wave current drive on ITER and future reactors, since single-pass damping in plasmas will be much higher because of their larger size and higher densities and temperatures. In addition, the simulation results that the driven current is comparable to the plasma current in experiment, confirm the viability of the coupled full wave and EK parameterization methods for FWCD.

Finally, we should point out that all the simulations are assumed Maxwellian distribution. Further studies of non-Maxwellian effects on FWCD and MCCD are still required, by means of coupling the full-wave method and a quasilinear Fokker-Planck solver developed by ourselves.

ACKNOWLEDGMENTS

The authors would like to thank Professor N. Xiang and B. J. Ding at the Institute of Plasma Physics, Chinese Academy of Sciences (ASIPP) and J. Q. Li at the Southwestern Institute of Physics (SWIP) for our fruitful discussions, and the Max Planck Institute for Plasma Physics (IPP) for providing the TORIC code. This work was supported by National Natural Science Foundation of China (Grant Nos. 11675073, 11575239, 11475083, and 11605088), Hunan Provincial Natural Science Foundation of China (Grant No. 2015JJ4044), the construct program of fusion and plasma physics innovation team in Hunan province (NHXTD03) and the Dr startup Funds of University of South China (No.2015XDQ43). It is worthy to mention that the equilibrium we used for the discharge #62946 at 2.8 s was kinetically EFITed by Professor Guoqiang Li and his student Kai Li with the experimental data of the plasma parameters provided by Professor Haiqing Liu, Bo Lv, and their diagnostic colleagues.

[1]C. C. Petty, F. W. Baity, J. S. deGrassie, T. K. Mau, R. I. Pinsker, M. Porkolab, and R. Prater, Plasma Phys. Controlled Fusion **43**, 1747 (2001).
[2]J. Hosea, R. E. Bell, B. P. LeBlanc, C. K. Phillips, G. Taylor, E. Valeo, J. R. Wilson, E. F. Jaeger, P. M. Ryan, J. Wilgen, H. Yuh, F. Levinton, S. Sabbagh, K. Tritz, J. Parker, P. T. Bonoli, R. Harvey, and NSTX Team. Phys. Plasmas **15**, 056104 (2008).
[3]R. I. Pinsker *et al.*, Nucl. Fusion **46**, 416–424 (2006).
[4]M. Ono, Phys. Plasmas **2**, 4075 (1995).
[5]M. Brambilla, Plasma Phys. Controlled Fusion **35**, 141 (1993).
[6]R. Majeski, J. H. Rogers, S. H. Batha, R. Budny, and E. Fredrickson, Phys. Rev. Lett. **76**, 764–767 (1996).
[7]A. Parisot, S. J. Wukitch, P. Bonoli, M. Greenwald, A. Hubbard, Y. Lin, R. Parker, M. Porkolab, A. K. Ram, and J. C. Wright, Plasma Phys. Controlled Fusion **49**, 219–235 (2007).
[8]Ye. O. Kazakov, V. G. Kiptily, S. Sharapov, D. Van Eester, and JET EFDA Contributors, Nucl. Fusion **52**, 094012 (2012).
[9]P. Jacquet, V. Bobkov, M. Mayoral, I. Monakhov, A. Scarabosio, I. Stepanov, M. Vrancken, and E. Wolfrum, Nucl. Fusion **52**, 042002 (2010).
[10]C. C. Petty, F. W. Baity, J. S. deGrassie, C. B. Forest, T. C. Luce, T. K. Mauc, M. Murakamia, R. I. Pinsker, P. A. Politzer, M. Porkolab, and R. Prater, Nucl. Fusion **39**, 1421 (1999).
[11]R. I. Pinsker, M. Porkolab, W. W. Heidbrink, Y. Luo, C. C. Petty, R. Prater, M. Choi, D. A. Schaffner, F. W. Baity, E. Fredd, J. C. Hosea, R. W. Harvey, A. P. Smirnov, M. Murakami, and M. A. Van Zeeland, Nucl. Fusion **46**, 416 (2006).
[12]R. I. Pinsker, M. E. Austin, S. J. Diem, E. J. Doyle, B. A. Grierson, J. C. Hosea, G. L. Jackson, M. C. Kaufman, T. C. Luce, R. Maggiora, D. Milanesio, A. Nagy, R. Perkins, P. A. Politzer, M. Porkolab, P. M. Ryan, W. M. Solomon, G. Taylor, F. Turco, and L. Zeng, AIP Conf. Proc. **1580**(1), 183–186 (2014).
[13]F. Meo, M. Brambilla, J.-M. Noterdaeme, D. Hartmann, G. Pereverzev, O. Gruber, and ASDEX Upgrade Team, in *Proceedings of the 27th EPS Conference on Controlled Fusion and Plasma Physics* (ECA, Budapest, 2000), Vol. 24, pp. 1613–1616.
[14]Y. Wan and HT-7 Team, Nucl. Fusion **40**, 1057 (2000).
[15]J. Li, B. Wan, and the EAST Team and International Collaborators, Nucl. Fusion **51**, 094007 (2011).
[16]X. J. Zhang, Y. P. Zhao, B. N. Wan, Y. Z. Mao, S. Yuan, D. Y. Xue, L. Wang, J. Y. Ding, S. Q. Ju, C. M. Qin, C. H. Wang, J. S. Shen, Y. T. Song, Y. Lin, J. G. Li, Y. Chen, and EAST Group, in Proceedings of the 23rd IAEA Fusion Energy Conference (Daejeon, Republic of Korea, 2010),

see www-pub.iaea.org/mtcd/meetings/PDFplus/2010/cn180/cn180papers/exwp7-30.pdf.
[17]X. J. Zhang, Y. P. Zhao, B. N. Wan, X. Z. Gong, Y. Z. Mao, S. Yuan, D. Y. Xue, L. Wang, C. M. Qin, S. Q. Ju, Y. Chen, J. P. Qian, L. Hu, J. G. Li, Y. T. Song, Y. Lin, S. Wukitch, J.-M. Noterdaeme, R. Kumazawa, T. Seki, K. Saito, and H. Kasahara, Nucl. Fusion **52**, 032002 (2012).
[18]L. Xin-Xia, X. Nong, and G. Chun-Yun, Chin. Phys. Lett. **32**, 035202 (2015).
[19]X. X. Li, N. Xiang, and X. J. Shi, Phys. Plasmas **21**, 092510 (2014).
[20]C. Yang, P. T. Bonoli, and J. C. Wright, Plasma Phys. Controlled Fusion **56**/**12**, 125003 (2014).
[21]B. J. Ding, E. H. Kong, M. H. Li, L. Zhang, W. Wei, M. Wang, H. D. Xu, Y. C. Li, B. L. Ling, Q. Zang, G. S. Xu, X. F. Han, H. L. Zhao, and the EAST Team, Nucl. Fusion **53**, 113027 (2013).
[22]B. J. Ding, Y. C. Li, L. Zhang, M. H. Li, W. Wei, E. H. Kong, M. Wang, H. D. Xu, S. L. Wang, G. S. Xu, L. M. Zhao, H. C. Hu, H. Jia, M. Cheng, Y. Yang, L. Liu, H. L. Zhao, Y. Peysson, J. Decker, M. Goniche, L. Amicucci, R. Cesario, A. A. Tuccillo, S. G. Baek, R. Parker, P. T. Bonoli, F. Paoletti, C. Yang, J. F. Shan, F. K. Liu, Y. P. Zhao, X. Z. Gong, L. Q. Hu, X. Gao, B. N. Wan, J. G. Li, and EAST Team, Nucl. Fusion **55**, 093030 (2015).
[23]V. P. Bhatnagar, R. Koch, P. Geilfus, and R. Kirkpatrick, Nucl. Fusion **24**, 955 (1984).
[24]E. F. Jaeger, L. A. Berry, E. D'Azevedo, D. B. Batchelor, M. D. Carter, K. F. White, and H. Weitzner, Phys. Plasmas **9**, 1873 (2002).
[25]R. J. Dumont, Nucl. Fusion **49**, 075033 (2009).
[26]E. A. Lerche and P. U. Lamalle, AIP Conf. Proc. **787**, 234 (2005).
[27]M. Brambilla and T. Krücken, Nucl. Fusion **28**, 1813 (1988).
[28]M. Brambilla, Plasma Phys. Controlled Fusion **41**, 1 (1999).
[29]Y. Lin, S. Wukitch, P. T. Bonoli, E. Nelson-Melby, M. Porkolab, J. C. Wright, and N. Basse, Phys. Plasmas **11**, 2466 (2004).
[30]S. J. Wukitch, Y. Lin, A. Parisot, J. C. Wright, P. T. Bonoli, M. Porkolab, N. Basse, E. Edlund, A. Hubbard, L. Lin, A. Lynn, E. Marmar, D. Mossessian, P. Phillips, and G. Schilling, Phys. Plasmas **12**, 056104 (2005).
[31]M. Brambilla and R. Bilato, Nucl. Fusion **46**, 387 (2006).
[32]J. C. Wright, P. T. Bonoli, M. Brambilla, F. Meo, E. D'Azevedo, D. B. Batchelor, E. F. Jaeger, L. A. Berry, C. K. Phillips, and A. Pletzer, Phys. Plasmas **11**, 2473 (2004).
[33]P. T. Bonoli, M. Brambilla, E. Nelson-Melby, C. K. Philips, and M. Porkolab, Phys. Plasmas **7**, 1886 (2000).
[34]M. Choi, V. S. Chan, and R. I. Pinsker, Nucl. Fusion **46**, 409 (2006).
[35]D. A. Ehst, Nucl. Fusion **25**, 629 (1985).
[36]Ye. O. Kazakov, I. V. Pavlenko, and D. Van. Eester, Plasma Phys. Controlled Fusion **52**, 115006 (2010).
[37]D. A. Ehst, K. Evans, Jr., and D. W. Ignat, Nucl. Fusion **26**, 461 (1986).
[38]D. A. Ehst, Nucl. Fusion **31**, 1933 (1991).
[39]R. Bilato, M. Brambilla, I. Pavlenko, and F. Meo, Nucl. Fusion **42**, 1085–1093 (2002).
[40]Ye. O. Kazakov, D. Van Eester, E. Lerche, T. Wauters, and J. Ongena, in Proceedings of the 41st EPS Conference on Plasma Physics (2014), p. P2.0319.